AIAA JOURNAL
Vol. 42, No. 7, July 2004

Controller Complexity for Active Control of Turbulent Boundary-Layer Noise from Panels

Gary P. Gibbs,* Randolph H. Cabell,† and Jer-Nan Juang‡
NASA Langley Research Center, Hampton, Virginia 23681

An experimental study of feedback controller complexity vs noise reduction performance for active structural acoustic control of turbulent-boundary-layer (TBL)-induced sound radiation from a panel is described. The reduction of total radiated sound power as a function of the number of actuators, sensors, and controller cost function on a mock aircraft sidewall subjected to TBL excitation are discussed. The results demonstrate total radiated sound power reductions of 15 dB at resonances and 10 dB integrated over 150–1000 Hz for a three-actuator and 15-sensor case. The controller configuration was then simplified to one actuator and four sensors (summed outputs) and was found to produce 10–15-dB reductions in sound power at resonances and 9 dB integrated over the control bandwidth. This result demonstrates the potential for achieving significant reductions in radiated sound power with a relatively simple actuator/sensor topology.

Nomenclature

$\boldsymbol{A}, \boldsymbol{B}, \boldsymbol{C}, \boldsymbol{D}$	=	discrete-time state-space matrices
J	=	control objective function
$\boldsymbol{K}$	=	feedback gain matrix
k	=	current time index
m	=	number of control inputs
P	=	total radiated sound power
p	=	control horizon
q	=	future time index
$\boldsymbol{R}$	=	radiation matrix
r	=	number of control outputs
$\boldsymbol{u}_p$	=	vector of current and future controller outputs
$\boldsymbol{u}_p^{\text{opt}}$	=	optimal control input
$\boldsymbol{v}$	=	complex velocities of each elemental radiator on the panel
$\boldsymbol{x}$	=	state vector
$\boldsymbol{y}$	=	vector of current and future plant responses
$\boldsymbol{y}_p$	=	vector of current and future plant outputs
$\boldsymbol{\Gamma}_p$	=	system controllability matrix
$\boldsymbol{\Omega}_p$	=	system observability matrix
$\boldsymbol{\Upsilon}_p$	=	system Markov parameter matrix

Introduction

ACTIVE control methods have been proposed for noise control in aircraft in the low-frequency range because of their potential weight and size savings over conventional passive systems. Active control of tonal noise has been studied extensively over the last two decades. Commercial feedforward control systems are found on several types of commercial and general aviation propeller aircraft.

In contrast, turbulent-boundary-layer (TBL)-induced noise and jet noise are the dominant sources in high subsonic and supersonic aircraft. These sources are broadband in nature and much more difficult to control actively. TBL noise is nearly spatially and temporally incoherent, thus limiting the use of TBL pressure measurements as reference signals for feedforward control. These considerations have motivated research into feedback approaches for broadband control of sound radiation from lightly damped structures over the past few years.[1–3]

Guigou and Fuller[4] and Johnson et al.[5] have developed an alternative feedforward approach utilizing feedforward reference signals obtained from structural acceleration measurements. Radiation control is achieved at the structure/air interface through active foam elements.

Feedback control of TBL excited noise has been studied analytically[6]; however, there has been little experimental work in this area. An analytical study of feedback control of sound radiation caused by TBL was described by Thomas and Nelson[7] and later studied in an experiment with a simulated TBL excitation.[8] Other analytical work by Heatwole et al. simulated active control of TBL-induced sound radiation from a single panel.[9] Loop shaping by observing the closed-loop performance on a Nichols chart was required, thus limiting the usefulness to the low-modal-density (frequency) region. The analytical work presented by Maury et al.[6] agrees qualitatively well with the work presented in this paper.

Experimental studies of the TBL control problem have been helped by recent developments in multi-input/multi-output feedback control algorithms that can handle modally dense systems.[10] These approaches utilize time-domain, experimentally based design schemes, which are in contrast to the Laplace domain approaches covered by Cox et al.[2] and Baumann et al.[1]

In addition to controller development, methods for predicting sound radiation using structural measurements have seen substantial progress. Maillard and Fuller demonstrated a technique of processing signals from accelerometer arrays such that a time-domain estimate of sound radiation was predicted in a specific direction.[11] Elliott and Johnson[12] and Currey and Cunefare[13] demonstrated the benefits of describing sound radiation from planar structures in terms of orthogonal radiation components (radiation modes). This approach was further refined in the radiation-modal-expansion (RME) technique developed by Gibbs et al., which creates a reduced-order approximate model of the dominant radiation modes.[14] This allows the efficient real-time implementation of radiation mode estimates using conventional digital-signal-processing (DSP) hardware, surface vibration measurements, and was used to create the benchmark cost function for the control system used in this paper.

Recently Gibbs et al. demonstrated active control of turbulent boundary-layer-induced sound radiation from two aircraft panels using generalized predictive control and radiation filters.[15] They obtained reductions in sound radiation of 10–20 dB at resonances and 5–10 dB integrated from 150–800 Hz at flow speeds of Mach 0.8 and 2.5. The control system used three actuators and 15 sensors (to predict radiation) per panel bay. For control systems of this type to be feasible on commercial aircraft, with hundreds of

Received 30 October 2001; revision received 1 October 2003; accepted for publication 11 November 2003.

*Research Scientist, Structural Acoustics Branch. Member AIAA.
†Research Scientist, Structural Acoustics Branch.
‡Research Scientist, Structural Dynamics Branch. Fellow AIAA.

sidewall panels, the controller configuration will have to be simplified. It is the purpose of this paper to experimentally investigate the tradeoff between controller complexity and noise reduction performance. This tradeoff study was performed on a low-speed tunnel for simplicity and cost, but performance results are similar to those found in the previously published work by Gibbs et al.[15]

Controller Configuration

In the following sections the controller configurations and algorithms will be outlined. Exhaustive details of the control system theory will be omitted for brevity, but appropriate references are included where needed.

Generalized Predictive Control Algorithm

The control algorithm used for these tests was a generalized predictive controller,[16] which belongs to the family of model predictive controllers. The basic concept behind model predictive controllers is to use a separately identified plant model to predict the plant response a number of time steps into the future as a function of future control inputs and system outputs. The future control inputs are then optimized to produce a desired plant response.[17] Only the first computed control input is applied, however, and the process is then repeated at the next time step to compute a new control input.

The cost function under which the control inputs are optimized can take many forms. For the current work the quadratic cost used was

$$J = \sum_{j=q}^{p-1} \|\boldsymbol{y}(k+j)\|^2 + \lambda \sum_{j=0}^{p-1} \|\boldsymbol{u}(k+j)\|^2 \tag{1}$$

This cost depends on future system responses, $\boldsymbol{y}(k+j)$, from time q to $p-1$ steps into the future, and future control inputs, $\boldsymbol{u}(k+j)$, from the current time to $p-1$ steps into the future. The parameter λ in the cost function determines the importance of the control inputs relative to the system responses. For an m-input, r-output control system, the system response vector has dimensions $(m \times 1)$, and the control input is an $(r \times 1)$ vector. The horizon p is usually chosen to be several times longer than the rise time of the plant in order to ensure a stable feedback controller.[18] If the start of the prediction horizon q equals zero (current time), then as $p \to \infty$ the resulting controller approaches the steady-state linear quadratic regulator.[18]

It is generally much easier to compute the optimal control inputs corresponding to the cost in Eq. (1) than to solve for the optimal linear quadratic regulator. The resulting computational savings can be important when the plant is time varying and the optimal control has to be recomputed at each time step. The plant was assumed to be time invariant for the experiments described here; nonetheless, this assumption will be relaxed in future work, and hence the GPC algorithm was used for the current work.

State-space and dynamic output feedback controllers[18] were used in these experiments, but in the interests of brevity only the state-space form is described here. Consider the nth order, r-input and m-output discrete-time model of a time-invariant system:

$$\boldsymbol{x}(k+1) = \boldsymbol{A}\boldsymbol{x}(k) + \boldsymbol{B}\boldsymbol{u}(k), \qquad \boldsymbol{y}(k) = \boldsymbol{C}\boldsymbol{x}(k) + \boldsymbol{D}\boldsymbol{u}(k) \tag{2}$$

By repeated substitutions, the state-space model can be written for a future time step p as

$$\boldsymbol{x}(k+p) = \boldsymbol{A}^p\boldsymbol{x}(k) + \boldsymbol{\Gamma}_p\boldsymbol{u}_p(k)$$

$$\boldsymbol{y}_p(k) = \boldsymbol{\Omega}_p\boldsymbol{x}(k) + \boldsymbol{\Upsilon}_p\boldsymbol{u}_p(k) \tag{3}$$

where $\boldsymbol{u}_p(k)$ and $\boldsymbol{y}_p(k)$ are column vectors extending p time steps into the future (i.e., $\boldsymbol{u}_p(k) = [\boldsymbol{u}(k), \ldots, \boldsymbol{u}(k+p-1)]^T$) and where $\boldsymbol{\Upsilon}_p$ is[19]

$$\boldsymbol{\Upsilon}_p = \begin{bmatrix} \boldsymbol{D} & \boldsymbol{0} & \boldsymbol{0} & \cdots & \boldsymbol{0} \\ \boldsymbol{CB} & \boldsymbol{D} & \ddots & \ddots & \boldsymbol{0} \\ \boldsymbol{CAB} & \boldsymbol{CB} & \boldsymbol{D} & \ddots & \boldsymbol{0} \\ \vdots & \ddots & \ddots & \ddots & \boldsymbol{0} \\ \boldsymbol{CA}^{p-2}\boldsymbol{B} & \cdots & \boldsymbol{CAB} & \boldsymbol{CB} & \boldsymbol{D} \end{bmatrix} \tag{4}$$

Rewriting the plant response for an arbitrary future time step q yields

$$\boldsymbol{y}_p(k+q) = \boldsymbol{\Omega}_p\boldsymbol{x}(k+q) + \boldsymbol{\Upsilon}_p\boldsymbol{u}_p(k+q) \tag{5}$$

Equation (3) can be substituted here for $\boldsymbol{x}(k+q)$, which produces an expression for $\boldsymbol{y}_p(k+q)$ in terms of the current state $\boldsymbol{x}(k)$, and future control inputs. This result can then be substituted into the cost function, and the resulting quadratic form solved to yield the vector of optimal future control inputs

$$\boldsymbol{u}_p^{\text{opt}}(k) = -\left[\boldsymbol{\Upsilon}_p^T\boldsymbol{\Upsilon}_p + \lambda\boldsymbol{I}\right]^{-1}\boldsymbol{\Upsilon}_p^T\boldsymbol{\Omega}_p\boldsymbol{x}(k) \tag{6}$$

where q is assumed to be zero. Only the control inputs corresponding to time k are applied to the system, which correspond to the first r rows of $\boldsymbol{u}_p^{\text{opt}}(k)$. The net result is a full state feedback controller, where the control input at time k is given by

$$\boldsymbol{u}(k) = -\boldsymbol{K}\boldsymbol{x}(k) \tag{7}$$

The feedback gain matrix $\boldsymbol{K}$ is constant for a time-invariant system.

Controlling Radiated Sound Power

The goal of applying control was to reduce the total sound power radiated from the panel. Baumann et al.[1] described a method for formulating a feedback control problem using structural measurements for feedback instead of far-field microphone responses. The microphone responses would introduce excessive delay in the controller as a result of propagation time and thereby reduce controller performance. The approach taken here was similar to that of Baumann; however, instead of formulating the problem in terms of modal responses of the panel, Elliott and Johnson's[12] method of elemental radiators was used. This approach eliminates the requirements of an analytical structural model. This method relies on a discretization of the Rayleigh integral, whereby the panel is split into elemental sources, and the total radiated sound power computed using the expression

$$P(\omega) = \boldsymbol{v}^H(j\omega)\boldsymbol{R}(\omega)\boldsymbol{v}(j\omega)$$

where the vector $\boldsymbol{v}(j\omega)$ contains the complex velocities of each elemental radiator on the panel.

To implement control of radiated sound power, the properties of $\boldsymbol{R}$ must be incorporated into the controller, either in the cost function when the controller gains are designed (as per Cox et al.[2]) or computed directly at each time step, as was done in Gibbs et al.[15]

In either case, the properties of $\boldsymbol{R}$ must be compactly represented over the frequency range of interest. Unfortunately, for the setup described in this paper complete implementation of the $\boldsymbol{R}$ matrix up to 1 kHz would require approximately 450 states. Thus the RME technique[14] was used, in which $\boldsymbol{R}$ is factored using the singular value decomposition at a normalization frequency into a set of orthogonal radiation modes. A plot of the radiation modes at 5 Hz is shown in Fig. 1. These modes are then used as a basis for $\boldsymbol{R}$ over the entire frequency range. The result is a set of radiation mode shapes, which are linear combinations of accelerometer outputs, plus a low-order frequency varying term for each mode that describes the mode's contribution to $\boldsymbol{R}$ at each frequency. Further model reduction is possible through implementation of only the radiation modes that are strong radiators over the bandwidth. This approach is an approximation, whose accuracy degrades away from the normalization frequency. However the errors are small over the bandwidth, and the method

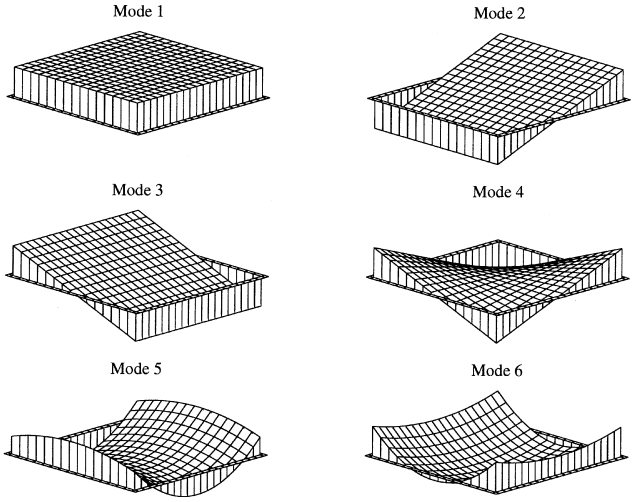

Fig. 1 Radiation modes for plate at 5 Hz.

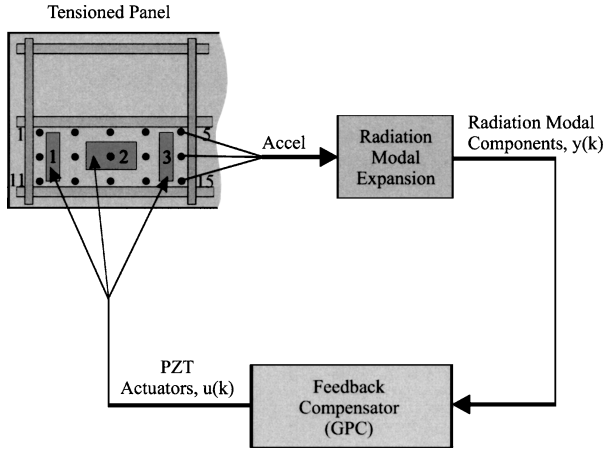

Fig. 2 Schematic of controller.

has proven useful for feedback control of panel radiation.[15] This method reduces the number of states needed (18 states) to model $\boldsymbol{R}$ by a factor of 25 compared to the case where the full $\boldsymbol{R}$ matrix is modeled (450 states). This complexity reduction permits its implementation on typical DSP hardware.

For these tests the normalization frequency was chosen to be 10 Hz, and the first six radiation modes were included in the modal expansion. Frequency variation for the RME technique was modeled using a third-order IIR filter, and the net result was a 15-input, 6-output state-space system with 18 states that transformed the time domain responses of 15 accelerometers into time-domain responses of six radiation modes.

A control system using this approach is shown diagrammatically in Fig. 2. Accelerometer responses were sampled and then passed through the radiation mode filters to produce time-domain responses of the radiation modes of interest. These radiation mode estimates were used in the feedback loop of the controller to compute the control inputs to the lead zirconium titanate (PZT) type of piezoceramic actuators.

System Identification

System identification was done using a time-domain method known as observer/Kalman-filter identification (OKID).[20] OKID computes system matrices $\boldsymbol{A}$, $\boldsymbol{B}$, $\boldsymbol{C}$, and $\boldsymbol{D}$ from time-domain input/output data and computes an observer gain matrix $\boldsymbol{L}$, which is needed to estimate the state vector $\boldsymbol{x}(k)$. OKID computes observer Markov parameters from time-domain input/output data, and from these extracts the system Markov parameters and observer gain Markov parameters. The order of the identified state-space model is usually specified to be four or five times higher than the true system order, in order to accurately identify the observer gain matrix.[20]

The input/output time histories were collected by driving the control actuators with broadband random signals and measuring the accelerometer responses. The accelerometer responses were then filtered through the radiation modal response model to produce time-domain responses of the six radiation modes. OKID was then used to build a state-space model from the PZT inputs to radiation mode outputs. Filtering the accelerometer responses through the radiation model does consume controller resources and introduces a phase shift into the system; however, the radiation model implements modal filtering on the raw accelerometer responses. It is easier and uses less states to identify from the PZT's to the estimated sound power (using RME) instead of identifying the structural plant only and then appending the radiation filters.

The input/output data were collected with the disturbance on, which reduced the coherence from the PZT inputs to radiation mode responses, but allowed OKID to build an internal model of the panel radiation response to the tunnel disturbance. This greatly improves the performance of the controller when the disturbance response is not white. A discussion of the characteristics of this internal noise model are beyond the scope of this paper, but it is discussed in Refs. 20 and 21.

Experimental Setup

The series of tests outlined in this paper were conducted in the Structural Acoustic Flow Apparatus (SAFA) at NASA Langley Research Center. SAFA is a low-speed wind tunnel capable of flow speeds up to Mach 0.23 with a test section of 50.8 cm × 50.8 cm. A photograph of the tunnel with the test panel removed is shown in Fig. 3, where the flow direction is from right to left.

To simulate aircraft construction, a tensioned panel assembly was built. The aluminum test panel was 1.5 mm thick, with dimensions of 152.4 cm in the flow direction and 50.8 cm in the crossflow direction. The panel replaced the sidewall of the tunnel in the open area shown in Fig. 3. The test panel had two vertical frames and one horizontal stringer, which partitioned the panel into six frame bays, each with dimensions 50.8 cm × 25.4 cm. The frames and stringers are similar to those found on a commercial aircraft. The panel was tensioned in the crossflow direction only to simulate the hoop stress caused by flight pressurization at 12.2 km. The longitudinal tension was omitted for simplicity.

Only the lower center bay, shown in Fig. 4, was used for this study. The baseline control configuration consisted of three piezoelectric (PZT) actuators (15.24 cm × 10.16 cm × 0.381 mm) and 15 accelerometers (Endevco 2250A-10). These lightweight (0.4 g) accelerometers have been shown to have a negligible effect on panel dynamics. Each actuator was centered about the horizontal centerline of the panel and hence was unable to drive even panel modes in the vertical direction. Preliminary tests showed that the panel response is dominated by modes with indices in the flow direction. The first panel mode with mode order 2 in the vertical direction does not occur until 553 Hz [(1,2) mode; see next section]. The three PZTs were arranged symmetrically about the vertical centerline of the panel, as can be seen in Fig. 4. The accelerometers were distributed on the panel in order to sense elemental velocities for the discretized Rayleigh integral method[12] providing an accurate estimate of total radiated sound power. These accelerometer signals were also sent to the control system, which utilized the aforementioned radiation-modal-expansion scheme to estimate the dominant radiation in real time.[14] The 50.8 cm × 25.4 cm panel was broken up into a 5 × 3 grid of equal areas, and an accelerometer was located at the center of each elemental area. Nine additional accelerometers were mounted on the frames and stringer around the panel to measure structural motions surrounding the test bay. The accelerometers are shown as * in Fig. 5, for example.

The feedback control algorithm was implemented on three Texas Instruments TMS320C40 digital signal processors hosted in a personal computer. The control system operated at a sample rate of 3 kHz for all of the tests described here. Antialiasing and reconstruction filters were set to 1 kHz. Closed- and open-loop performance

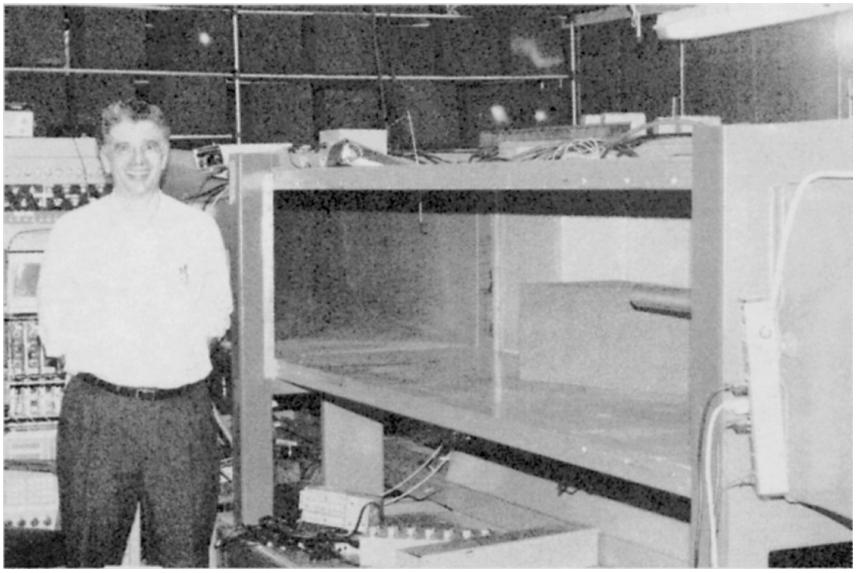

Fig. 3 Photograph of wind tunnel.

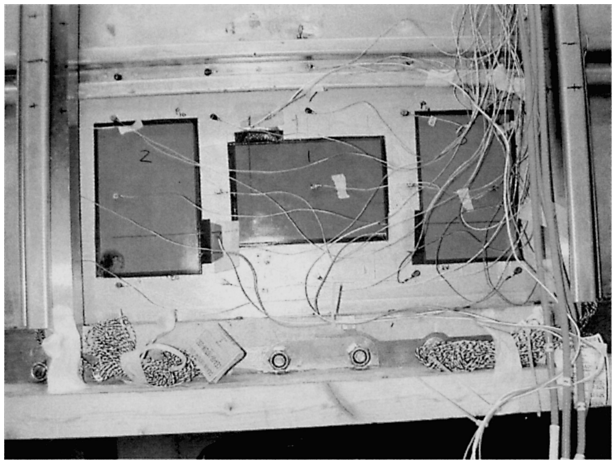

Fig. 4 Photograph of test panel.

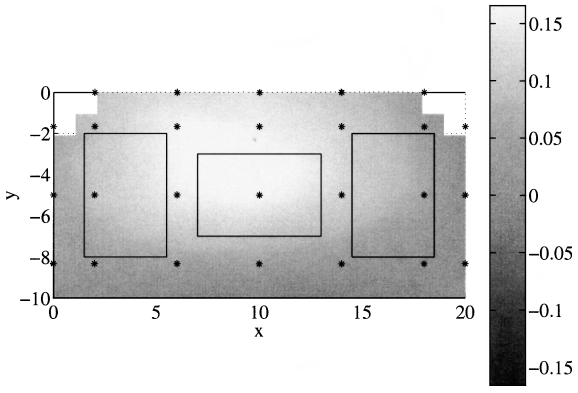

Fig. 5 Operating deflection shape at 180 Hz.

data were collected with an HP VXI data-acquisition system that was independent of the control system. The acquisition system sampled the accelerometer responses at 5120 Hz, from which the radiated sound power was computed. With this arrangement, it was possible to measure the controller performance over its entire bandwidth of 0–1500 Hz.

Experimental Results

Two series of tests were conducted to evaluate different control configurations. The controller performance as a function of the number of actuators was studied first, and a single actuator was chosen based on the results of these tests. Then, using the single actuator, different sensing configurations were studied. In all cases the performance was quantified using total radiated sound power calculated from the 15 accelerometer responses. Certainly more complicated radiation filters could be appended to include radiation into an actual aircraft cabin, but is beyond the scope of this work. More complex radiation models will be addressed in a future flight test. This section begins with a discussion of tunnel and controller characterization data. The data include microphone TBL measurements, the open-loop response of the panel, and the measured transfer function from the center PZT to the response of the first radiation mode.

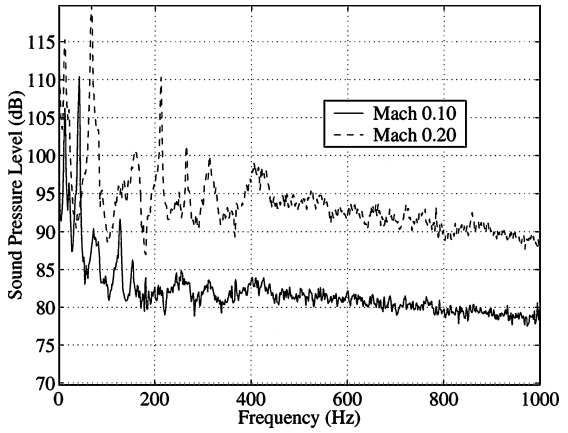

Fig. 6 Turbulent boundary-layer autospectrum measured upstream of the test panel (dB re. 20E–6 Pa).

The TBL spectrum was measured using B&K microphones flush mounted just upstream of the test panel. Typical autospectra of the upstream microphone for Mach 0.1 and 0.2 flow conditions are shown in Fig. 6. The autospectrum for the Mach 0.1 test condition is relatively smooth above 200 Hz. For the Mach 0.2 condition, the autospectrum is relatively smooth above 400 Hz. Below these frequencies the tunnel suffers from high background noise. Other characterization work in this wind tunnel proved that the tunnel acoustic noise is insignificant above these frequencies. Because of this low-frequency background noise, most of the results were measured at the Mach 0.1 condition, although the performance of the control system was verified at the Mach 0.2 condition.

Measurement uncertainty is an important aspect of experimentation. In this work we are concerned with the quantification of the reduction in radiated sound power as a result of active noise control

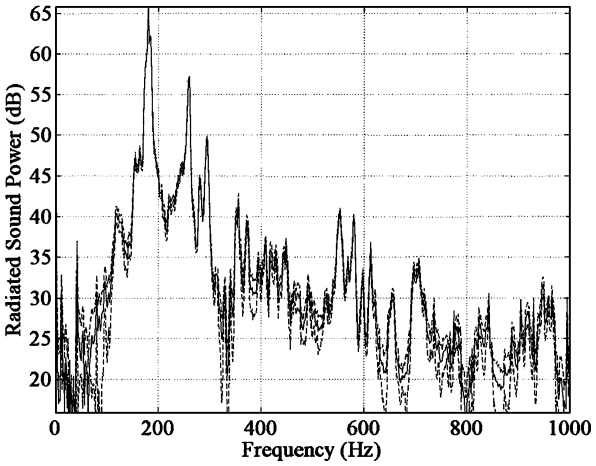

Fig. 7 Open-loop radiated sound power at Mach 0.1 (dB re. 1E–12 W).

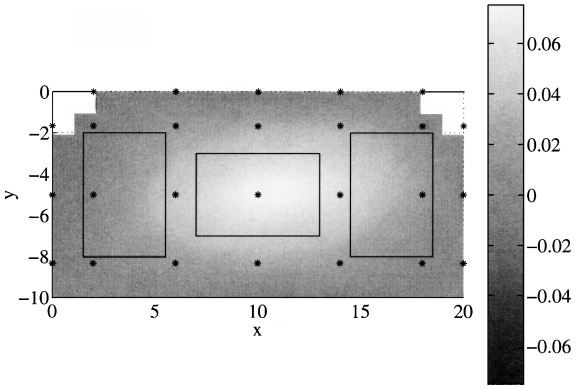

Fig. 8 Operating deflection shape at 258 Hz.

treatments. It is thus important that the dominant sound radiation metrics and overall trends provide consistent results. Unless otherwise specified in this paper, the uncertainty of all measured data is estimated by the small sample method of Kline and McClintock using assumed odds of 20:1 (Ref. 22). Based on manufacturer data sheets and experience with this type of accelerometer, the uncertainty of the accelerometer measurement is assumed to be $\pm 0.002g$ at 20:1 odds. Thus, the sound power radiated from the panel at Mach 0.1 is shown in Fig. 7 including confidence bounds (20:1). As can be seen in the figure, the radiated sound power is dominated by system resonances. The total radiated sound power is 73.8 ± 0.15 dB.

Accelerometer response plots at a single frequency (operating deflection shape) provide additional insight into the open-loop panel dynamics. The operating deflection shapes are not exactly equivalent to classic plate modes; however, the nearest classic plate mode designation will be used for reference. Resonances of the panel can be seen at 258 Hz [(1,1) mode], 295 Hz [(2,1) mode], 355 Hz [(3,1) mode], and at other frequencies. The strongest response in the figure, at 180 Hz, corresponds to a breathing mode of the upper and lower panels combined. A plot of the magnitude of the operating deflection shape at 180 Hz is shown in Fig. 5. The color white denotes the maximum positive deflection, and the color black denotes the maximum negative deflection. The black squares in the plot denote PZT locations, and the smaller stars, $*$, denote accelerometer locations. The accelerometers in the top row are on the stringer separating the upper and lower panels; similarly, the left-most and right-most accelerometers are on the frame surrounding the panel. Note that at 180 Hz the response appears to be dominated by the (1,1) panel resonance; however, the upper stringer is moving as well. The true (1,1) panel mode appears to be at 258 Hz, the response of which is shown in Fig. 8. Here, the frames and stringers are not moving, and the panel appears to be moving in the motion of a breathing mode of a single panel.

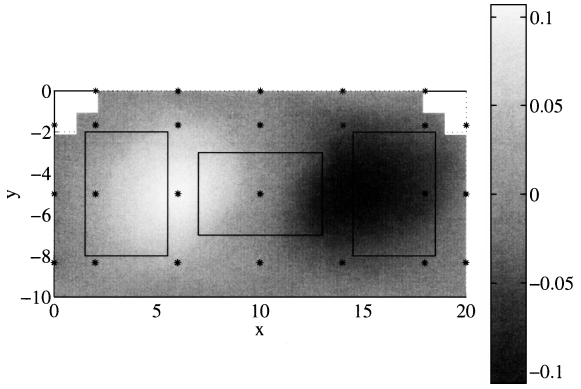

Fig. 9 Operating deflection shape at 295 Hz.

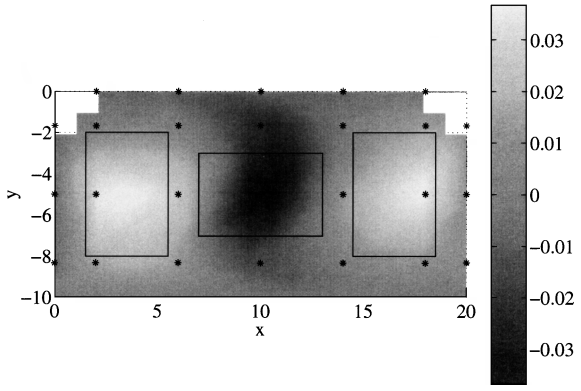

Fig. 10 Operating deflection shape at 355 Hz.

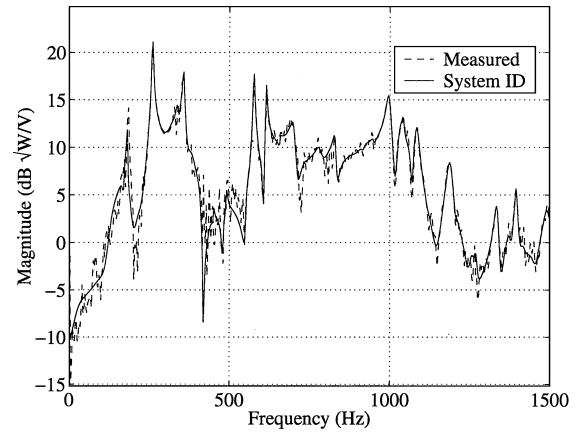

Fig. 11 Transfer function of center PZT to radiation mode 1 (typical).

More complicated operating deflection shapes are seen at higher frequencies. For example, the response plot at 295 Hz shown in Fig. 9 displays a clear (2,1) panel response, with the center PZT mounted on a node between the antinodes. A (3,1) panel mode is evident at 355 Hz, shown in Fig. 10. A (1,2) panel mode occurs at 553 Hz (vertically asymmetric), and this mode is uncontrollable by the actuators (vertically symmetric). At the slightly higher frequency of 580 Hz, the panel responds in a (2,2) mode, which is also uncontrollable. And finally, the panel response at 655 Hz corresponds to a (3,2) panel mode. In summary, the acoustic radiation from the aircraft style panels used in this experiment is dominated by low-order odd-odd structural bay modes, which radiate predominantly through the first radiation mode.

Measured and modeled transfer functions from the center PZT input voltage to the response of the first radiation mode, which is the dominant radiator below 500 Hz, are shown in Fig. 11. A six-output three-input state-space model, with 210 states, was fitted to measured data using the OKID procedure. The curve shows only one of the input-output paths in that model. The three resonances

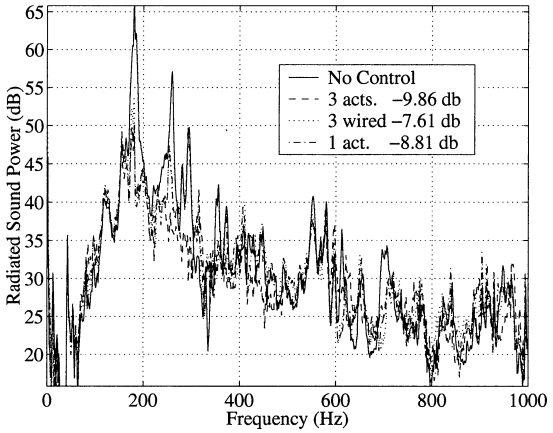

Fig. 12 Controller performance vs number of actuators.

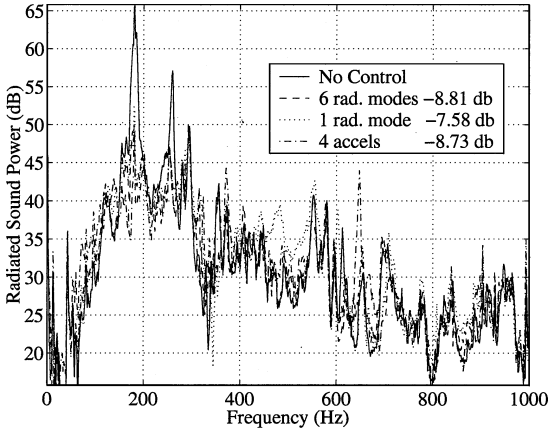

Fig. 13 Controller performance vs sensor complexity.

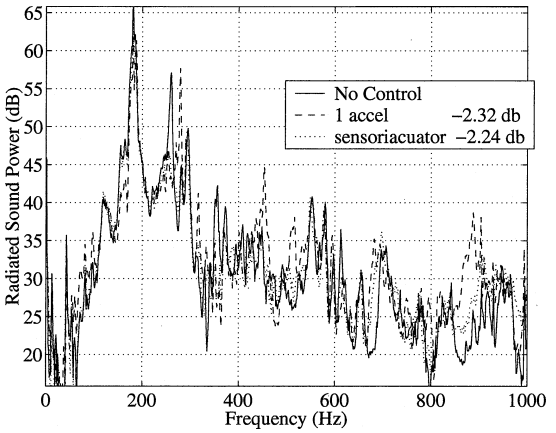

Fig. 14 Controller performance for single accelerometer and sensoriactuator.

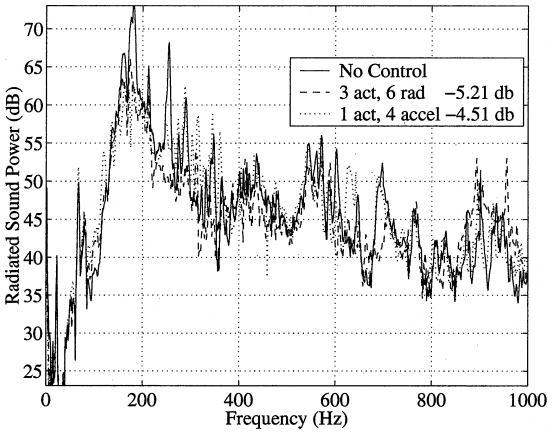

Fig. 15 Controller performance at Mach 0.20.

below 500 Hz correspond to a breathing mode of the upper and lower bays at 180 Hz, the (1,1) mode of the lower panel at 258 Hz, and the (3,1) panel mode at 355 Hz.

For the first series of tests (actuator complexity), the controller cost function included the responses of the first six radiation modes computed from the outputs of the 15 accelerometers. Three actuator configurations were tested: three actuators driven independently (three acts), three driven as one (three wired), and the center actuator driven alone (one act). Control and no control results for the three cases, in terms of total radiated sound power, are shown in Fig. 12. The solid curve corresponds to the open-loop condition (shown in Fig. 7), and the three remaining curves are the three actuator configurations. Uncertainty bounds show similar trends to those presented in Fig. 7 and are omitted for clarity. The main concern of this experiment is to determine relative performance of controllers as determined by their total radiated sound power. The total radiated sound power for each case is integrated from 150 to 1000 Hz and is displayed as reduction in decibels relative to the no-control case. It can be seen that all three configurations exhibit excellent performance with reductions of over 15 ± 0.61 dB at resonances and over 7.5 ± 0.71 dB integrated over the bandwidth (150–1000 Hz). There is no appreciable spillover above 1000 Hz. Based on these results, the single center actuator was down selected for further study.

In the next series of tests, only the center actuator was used, and five sensing strategies were examined: six radiation modes, one radiation mode, four accelerometers (3, 7, 9, and 13) in a diamond arrangement wired as one sensor, the center accelerometer (8), and the output of the center actuator configured as a sensoriactuator.[3] The sensoriactuator is a single transducer that is configured to act simultaneously as an actuator and sensor. The radiated sound power corresponding to the first three sensing configurations is shown in Fig. 13. Again the uncertainty bounds are similar to those shown in Fig. 7 and are omitted for clarity. All three strategies performed similarly with reductions at resonances on the order of 15 ± 0.52 dB and integrated reductions of over 7.5 ± 0.63 dB. The main differences are that the four-accelerometer case showed some spillover at 650 Hz, and the one-radiation mode case showed spillover between 450 and 550 Hz. There is no appreciable spillover above 1000 Hz.

Control performance for the remaining two cases is shown in Fig. 14. In both of these cases, the radiated sound power was reduced by 10 ± 0.20 dB at a couple of dominant modes and by 2.24 ± 0.27 dB for the single accel and 2.32 ± 0.26 dB for the sensoriactuator integrated over the bandwidth of 150 to 1000 Hz. Examination of the closed-loop operating deflection shape at 180 Hz for the single accelerometer case showed that the controller was able to pin the plate in the center. The plate still had significant response around the actuator. In other words, the single accelerometer signals suffers because of its point measurement. The most efficient sensing strategy would be a single distributed radiation mode one sensor. For the sensoriactuator case the controller was able to "whiten" the sensoriactuator signal resulting in little control of the dominant 180-Hz mode. This is because of the low controllability of the 180-Hz mode and the difficulty associated with separating the sensor signal and the larger actuator drive voltage.

After examining the results for all of the tests at Mach 0.1, the configuration consisting of the center PZT and the diamond arrangement of accelerometers seemed to be the best compromise in terms of controller complexity vs performance. This is in agreement with earlier results, which found that minimizing the volume velocity of a panel gives good results.[23]

Additional tests were performed at Mach 0.2 with the three-actuator/six-radiation mode configuration, and with a single actuator and only four accelerometers. The results are presented in Fig. 15. Again the uncertainty bounds are similar to Fig. 7 and are omitted for clarity. The increase in excitation shown in Fig. 6 resulted in an increase in radiated sound power of approximately 10 dB over the

entire bandwidth. For both cases the controller reduces the dominant resonances by approximately 10–15 $\pm$ 0.12 dB and results in a integrated reduction of 4.51 $\pm$ 0.18 dB and 5.21 $\pm$ 0.19 dB for the two cases, respectively. There is no appreciable spillover above 1000 Hz. Additional control performance is achievable; however, the authors limited the control voltages to approximately 75 Vrms for this test to prevent possible damage to the PZT actuators. The authors note as mentioned earlier that the acoustic pressure excitation is dominated by drive noise for frequencies below 400 Hz at this flow speed.

Conclusions

Experiments on the active control of sound radiation from a panel excited by a turbulent boundary layer have been described. Several actuation and sensing arrangements were tested to establish useful simplifications to the baseline control configuration which consisted of three piezoelectric (PZT) actuators and 15 accelerometers for estimating radiated sound power as a result of the first six radiation modes of the panel. A generalized predictive feedback control algorithm was used to generate control inputs to the PZT actuators.

Three actuator configurations were tested: three PZTs driven independently, three PZTs driven as a single actuator, and the center PZT by itself. All 15 accelerometers were used for these tests. The acoustic radiation from the aircraft style panels used in this experiment is dominated by low-order odd-odd structural bay modes that radiate predominantly through the first radiation mode. Reducing the number of actuators from three to one was found to have little effect on the overall reduction of total radiated sound power (9.9 $\pm$ 0.71 vs 8.8 $\pm$ 0.61 dB) and would appear to be a good tradeoff.

The best sensing strategy relies on being able to observe the first radiation mode with minimal spillover to other radiation modes. A good compromise sensing strategy utilizing four accelerometers arranged in a diamond pattern whose outputs are summed proved to be quite effective. Reductions of total radiated sound power of 8.7 $\pm$ 0.63 dB were achieved compared to 8.8 $\pm$ 0.61 dB for the six-radiation mode case. Thus, this arrangement with one actuator and a single group of four accelerometers is the best compromise in terms of performance vs controller complexity. The single-input/single-output (SISO) single accelerometer cases had relatively poor performance because of their lack of distributed sensing (promoting spillover). The SISO sensoriactuator case suffers in performance because of the relatively low controllability of the dominant mode (at 180 Hz). This low controllability creates difficulty in pulling the desired sensing signal out of the noise. These results are encouraging for flight implementation because the single PZT only adds 10% to the mass of the panel, but provides substantial reduction of the low frequency radiation.

References

[1]Baumann, W. T., Saunders, W. R., and Robertshaw, H. H., "Active Suppression of Acoustic Radiation from Impulsively Excited Structures," *Journal of the Acoustical Society of America*, Vol. 90, No. 6, 1991, pp. 3202–3208.

[2]Cox, D., Gibbs, G., Clark, R., and Vipperman, J., "Experimental Robust Control of Structural Acoustic Radiation," *Journal of Vibration and Acoustics*, Vol. 121, 1999, pp. 433–439.

[3]Vipperman, J. S., and Clark, R. L., "Multivariable Feedback Active Structural Acoustic Control Using Adaptive Piezoelectric Sensoriactuators," *Journal of the Acoustical Society of America*, Vol. 105, No. 1, 1999, pp. 219–225.

[4]Guigou, C., and Fuller, C., "Control of Aircraft Interior Broadband Noise with Foam-PVDF Smart Skin," *Journal of Sound and Vibration*, Vol. 220, No. 3, 1999, pp. 541–557.

[5]Johnson, M. E., Griffin, J., and Fuller, C. R., "Experiments on Feedforward Control of Turbulent Boundary Layer Noise," *Proceedings of Active-99*, edited by S. Douglas, Inst. of Noise Control Engineering, Washington, DC, 1999, pp. 435–445.

[6]Maury, C., Gardonio, P., and Elliott, S., "Active Control of the Flow-Induced Noise Transmitted Through a Panel," *AIAA Journal*, Vol. 39, No. 10, 2001, pp. 1860–1867.

[7]Thomas, D., and Nelson, P., "Feedback Control of Sound Radiation from a Plate Excited by a Turbulent Boundary Layer," *Journal of the Acoustical Society of America*, Vol. 98, No. 5, 1995, pp. 2651–2662.

[8]Thomas, D., and Nelson, P., "Experiments on the Active Control of Broadband Sound Radiation from a Lightweight Partition," *Journal of Sound and Vibration*, Vol. 202, 1997, pp. 438–445.

[9]Heatwole, C. M., Franchek, M. A., and Bernhard, R. J., "Robust Feedback Control of Flow-Induced Structural Radiation of Sound," *Journal of the Acoustical Society of America*, Vol. 102, No. 2, 1997, pp. 989–997.

[10]Juang, J.-N., and Eure, K. W., "Predictive Feedback and Feedforward Control for Systems with Unknown Disturbances," NASA Tech. Rep. TM-208744, May 1998.

[11]Maillard, J. P., and Fuller, C. P., "Advanced Time Domain Wave-Number Sensing for Structural Acoustic Systems. I. Theory and Design," *Journal of the Acoustical Society of America*, Vol. 95, No. 6, 1994, pp. 3252–3261.

[12]Elliott, S. J., and Johnson, M. E., "Radiation Modes and the Active Control of Sound Power," *Journal of the Acoustical Society of America*, Vol. 94, No. 4, 1993, pp. 2194–2204.

[13]Currey, M. N., and Cunefare, K. A., "The Radiation Modes of Baffled Finite Plates," *Journal of the Acoustical Society of America*, Vol. 98, No. 3, 1995, pp. 1570–1580.

[14]Gibbs, G. P., Clark, R. L., Cox, D. E., and Vipperman, J. S., "Radiation Modal Expansion: Application to Active Structural Acoustic Control," *Journal of the Acoustical Society of America*, Vol. 107, No. 1, 2000, pp. 332–339.

[15]Gibbs, G. P., Eure, K. W., and Lloyd, J. W., "Active Control of Turbulent Boundary Layer Induced Sound Radiation from Aircraft Style Panels," *Proceedings of Active-99*, edited by S. Douglas, Inst. of Noise Control Engineering, Washington, DC, 1999.

[16]Clarke, D., Mohtadi, C., and Tuffs, P., "Generalized Predictive Control—Part I. The Basic Algorithm," *Automatica*, Vol. 23, No. 2, 1987, pp. 137–148.

[17]Garcia, C. E., Prett, D. M., and Morari, M., "Model Predictive Control: Theory and Practice—A Survey," *Automatica*, Vol. 25, No. 3, 1989, pp. 335–348.

[18]Mosca, E., *Optimal, Predictive, and Adaptive Control*. Prentice–Hall, Upper Saddle River, NJ, 1995, Chap. 1.

[19]Phan, M. Q., Lim, R. K., and Longman, R. W., "Unifying Input–Output and State-Space Perspectives of Predictive Control," Dept. of Mechanical and Aerospace Engineering, TR 3044, Princeton Univ., Princeton, NJ, Sept. 1998; also *Journal of Vibration and Control* (to be published).

[20]Juang, J.-N., *Applied System Identification*, Prentice–Hall, Upper Saddle River, NJ, 1994, Chap. C.

[21]Goodzeit, N. E., and Phan, M. Q., "System Identification in the Presence of Completely Unknown Periodic Disturbances," *Journal of Guidance, Control, and Dynamics*, Vol. 23, No. 2, 2000, pp. 251–259.

[22]Kline, S. J., and McClintock, F. A., "Describing Uncertainties in Single Sample Experiments," *Mechanical Engineering*, Vol. 75, No. 1, 1953, pp. 3–8.

[23]Johnson, M., and Elliott, S., "Active Control of Sound Radiation Using Volume Veclocity Cancellation," *Journal of the Acoustical Society of America*, Vol. 98, No. 4, 1995, pp. 2174–2186.

W. J. Devenport
Associate Editor